IEEE Access
Multidisciplinary ⋮ Rapid Review ⋮ Open Access Journal

Received 14 May 2024, accepted 27 May 2024, date of publication 30 May 2024, date of current version 14 June 2024.

Digital Object Identifier 10.1109/ACCESS.2024.3407371

RESEARCH ARTICLE

Machine Learning-Based Optimized 3G/LTE/5G Planar Wideband Antenna With Tri-Bands Filtering Notches

SULEIMAN ALIYU BABALE[1,4], (Member, IEEE), TAN KIM GEOK[1], (Member, IEEE), SHARUL KAMAL ABDUL RAHIM[2], (Fellow, IEEE), CHIA PAO LIEW[3], UMAR MUSA[4], (Student Member, IEEE), MUKHTAR FATIHU HAMZA[5], YASER AWADH BAKHURAISA[1], AND LI LI LIM[6], (Senior Member, IEEE)

[1]Faculty of Engineering and Technology, Multimedia University, Melaka 75450, Malaysia
[2]Wireless Communication Centre, Faculty of Electrical Engineering, Universiti Teknologi Malaysia, Skudai, Johor 81310, Malaysia
[3]School of Energy and Chemical Engineering, Xiamen University Malaysia, Sepang, Selangor 43900, Malaysia
[4]Department of Electrical Engineering, Bayero University Kano, Kano 3011, Nigeria
[5]Department of Mechanical Engineering, College of Engineering in Alkharj, Prince Sattam bin Abdulaziz University, Al-Kharj 11942, Saudi Arabia
[6]Faculty of Engineering and Technology, Tunku Abdul Rahman University of Management and Technology, Kuala Lumpur 53300, Malaysia

Corresponding authors: Tan Kim Geok (kgtan@mmu.edu.my) and Sharul Kamal Abdul Rahim (sharulkamal@fke.utm.my)

This work was supported in part by the Telecom Malaysia and Multimedia University under Grant MMUE/220012.

ABSTRACT A multiband microstrip-fed wideband (WB) antenna with filtering notches is described for 3G/4G/5G applications. The proposed antenna comprises three notch bands by etching a modified inverted U-slot, a square ring slot, and an interdigital inductor slot on the patch element and feedline. The antenna resonates at 1.9, 2.3, and 3.5 GHz due to the resonant components' mutual interaction, which eliminates interference at other frequencies. The antenna's measured S_{11} are 18.79 dB at 1.9 GHz, −24.8 dB at 2.4 GHz, and −40.6 dB at 3.5 GHz, showing a multiband function with a band-reject level of 0.4 dB. The VSWR is less than two at all resonant frequencies. The effects of altering the notch dimensions on the S_{11} and VSWR were explored. The antenna was developed and tested using a Rogers RT/Duroid 5880 substrate. The agreement between measured and simulated results was satisfactory. The S_{11} result was validated using the ADS schematic and machine learning techniques. The proposed triband-notched antenna offers encouraging results, with radiation patterns exhibiting omnidirectional characteristics and effective performance within the required frequencies. Current distribution analysis reveals how notches disrupt surface current and lower radiation at specific frequencies. The antenna's gain and efficiency performed satisfactorily in the stated frequency ranges.

INDEX TERMS Wideband antenna, interdigital inductor, radiating patch, multiband, split ring resonator, notch band.

I. INTRODUCTION

Antenna designs are facing increasing pressures due to the advancement and emergence of modern wireless technologies. In modern times, numerous systems employ multiple frequency bands, therefore requiring the employment of antennas that can operate over multiple bands [1], [2], [3], [4], [5], [6], [7]. Many different techniques are used to obtain multiband antennas [8]; one popular option is to design a single patch antenna responsive to numerous interesting frequencies. Such an antenna is built from a combination of several sections that when coupled will give the desired narrowed bands. The combination of various resonance components will inevitably result in a deterioration of performance when forming the multiband antenna, even though each narrowband resonant structure may individually demonstrate exceptional sensitivity to its narrowband resonant frequencies [9]. Additionally, narrowband resonant

The associate editor coordinating the review of this manuscript and approving it for publication was Bilal Khawaja.

components' mutual coupling is introduced. The efficacy of the desired modes may be decreased as a result of this coupling, which may also produce incorrect and unwanted modes of operation [10]. Wideband systems experience significant electromagnetic interference due to the presence of multiple nearby narrow-band systems, making it a critical factor to consider. For instance, a UWB antenna functions in the frequency range of 3.1-10.6 GHz, however, not all applications need the entire range to function. Many other applications may regard certain narrower bands to be interference. WiMAX, operating within the frequency range of 3.3 to 3.8 GHz, may perceive a WLAN operating in the spectrum of 5.15 to 5.825 GHz as a notable source of interference. To prevent any undesired frequencies from operating across the system, a wideband (WB) antenna covering the appropriate frequency range and incorporating some band notches is required as depicted in [11], [12], and [13].

An in-depth study has been done on wideband antennas with notch band capabilities [14], [15], [16], [17], [18], [19]. It has recently been shown that a rejected band within a broad operational bandwidth can be generated by appropriately etching several slots of different dimensions on the ground plane [20], the radiating patch [21], [22], [23], [24], [25], or both [26], [27], [28]. This band-reject action is achievable when the slot lengths are a multiple of λ_n, where λ_n represents the wavelength of the antenna at the notch frequency. In this instance, the antenna's stimulated surface currents will encounter destructive interference, rendering it unusable at that frequency. To create any kind of notch bands inside the wideband systems, resonant components are often added to the antenna. This entails inserting variously shaped slots into the antenna, including slots with the U-shape [24], inverted C-shape [29], H-shape [30], L-shape [31], and W or inverted M-shape [32], etc. Split-ring resonators (SRR) were employed in the antenna configuration by the authors of [33] and [34] to produce notch bands. A log periodic dipole antenna can also have rejection bands by including numerous U-shaped slots, as demonstrated in [35]. To make notch bands, the authors of [36] and [37] altered the U-slot on the monopole antenna.

Fig. 1, shows the sketch of an RF front-end system, from which Fig. 1(a) depicts the wideband antenna with three notch filters. Fig. 1(b) shows the proposed triband-notched antenna, from which the filters are replaced with some band notches within the antenna itself.

In this paper, a multiband antenna for 3G, 4G, and 5G applications was designed and implemented employing several notches on the patch. Initially, a wideband microstrip antenna was created utilizing defected ground and was expressly to cover only the targeted frequencies (2.0 GHz to 5.5 GHz). The notch-band antenna, in particular, was developed to be simple, planar, and without any via holes. By including three different types of slits on the radiating patch; a modified inverted U-slot, a square ring slot, and an interdigital inductor slot, the proposed antenna has

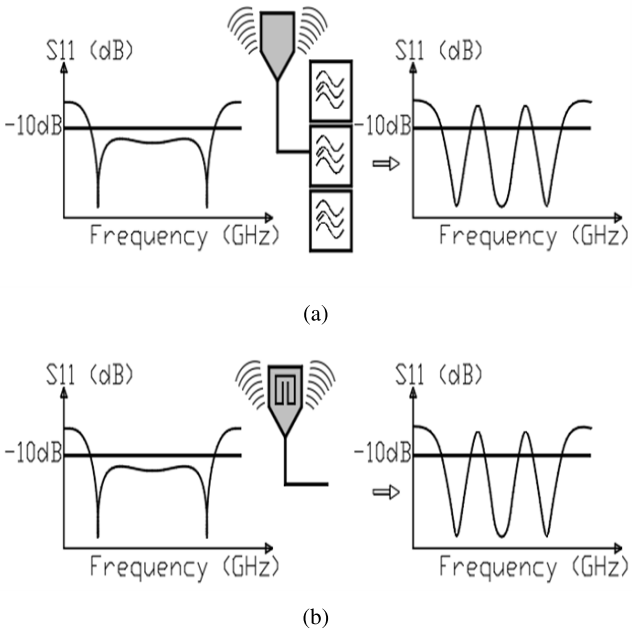

FIGURE 1. The RF front end system; (a) The three notch filters on the wideband antenna (b) the proposed triband-notched antenna.

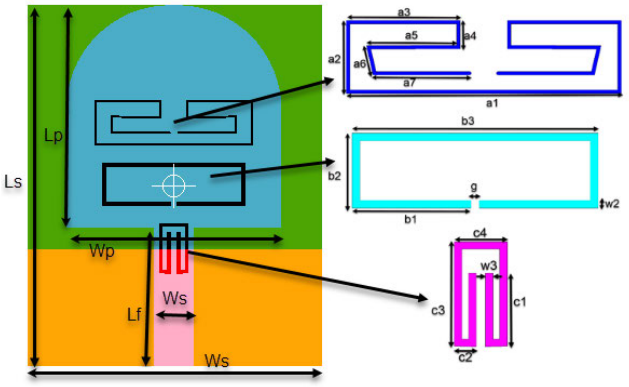

FIGURE 2. The structures of the proposed antenna incorporating the three notches.

band-notching capabilities that can eliminate interference from other frequencies within the range enabling the antenna to resonate at the targeted frequencies of 1, 9 GHz, 2.3 GHz and 3, 5 GHz. Fig. 2 depicts the proposed antenna's geometry. The lengths of the substrate and the patch are respectively, Ls and L_p. The width of the patch is specified as Wp, whereas the substrate width is Ws. width (Wf) and length (L_f) for the feedline. Subsequent sections will explore the various characteristics of the three notches dimensions.

The proposed antenna, in particular, was developed to be simple, planar, and without any via-holes. By including three different types of slits on the radiating patch; a modified inverted U-slot, a square ring slot, and an interdigital inductor slot, the proposed antenna has band-notching capabilities that can eliminate interference from other frequencies within the range enabling the antenna to resonate at the targeted frequencies of 1.9 GHz, 2.3 GHz, and 3.5 GHz. The

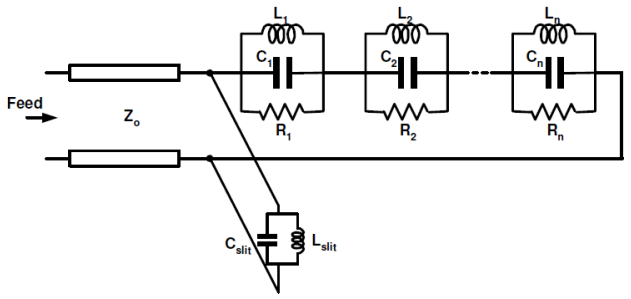

FIGURE 3. Impedance model for the WB antenna's radiating element.

configuration of the proposed antenna is displayed in Fig. 2, with Ls and Lp representing the lengths of the substrate and the radiating patch respectively. The width of the radiating patch is denoted by Wp, whereas the substrate width is Ws. width (Wf) and length (Lf) for the feedline. Subsequent parts will address the other aspects of the three notches dimensions.

II. RESEARCH CONTRIBUTION

The main contributions of this research article are itemized as follows:

- The proposed antenna was developed to be planar, simple, and without any via-holes.
- The antenna was developed to have triband notches with a notch depth level near 0 *dB*. which measured how much the frequency is rejected at the notch frequencies.
- In addition to the measurement validation, an equivalent circuit model of the proposed design was developed and presented as another means for validation.
- A Machine learning algorithm was used to predict the S_{11} and the efficiency curve. With this model, by arbitrarily assuming any sets of the input variables like the length, width, substrate specifications, and other notch filter parameters, the corresponding S_{11} curve could be approximately determined without using a 3D Full-wave EM-Field Simulation tools like CST, HFSS, FEKO or any antenna design software.

III. ANTENNA MODEL

The proposed wideband antenna's equivalent circuit, depicted in Fig. 3, has a band-notched design with many RLC parallel cells stacked in series to approximate the radiating element.

The equivalent circuit of the input impedance is expressed as follows [38]:

$$Z_n = \sum_{i=1}^{n} \left(\frac{j\omega R_i L_i}{R_i \left(1 - \omega^2 C_i L_i\right) + j\omega L_i} \right) \tag{1}$$

where Zn is the input impedance, R_i, L_i and C_i are the resistance, inductance, and capacitance that form the parallel RLC resonant circuit respectively. The angular frequency is represented as Ω. The simplified expressions for the parallel resistance, inductance, and capacitance are given as [39] and that of the reflection coefficient (S_{11}) from [27]:

$$L = \frac{\mathrm{Im}\,(Z_{11})}{2\pi f} \tag{2}$$

$$C = \frac{1}{(2\pi f)^2 L} \tag{3}$$

$$f = \frac{1}{2\pi f \sqrt{LC}} \tag{4}$$

$$S_{11} = \frac{Z_n - Z_0}{Z_n + Z_0} \tag{5}$$

Two goals were taken into account while designing the 3-notched band antenna. The first step is to design an antenna capable of covering a wide bandwidth. The second is to add notch structures to the antenna to eliminate interference that may arise throughout the entire operating frequency. To this aim, the following sections cover the wide-band antenna design and each notch's integration.

A. WIDE-BAND ANTENNA DESIGN

The design was conducted on a 1.58 mm-height Rogers RT/Duroid5880 substrate, which had a tangent loss of 9×10^{-4} and a relative permittivity $\varepsilon_r = 2.2$. The extended length of the fringing field was designated as $\sim$ L, the patch's width and length as 'Lp' and 'Wp,' respectively, and the effective permittivity $\varepsilon_{\mathrm{eff}}$. The dimensions of the patch are calculated using the following formulae [40]. By using equations provided in [40], the physical parameters of the antenna were obtained and the optimized values are; $\mathrm{W_p} = 18.6$ mm, $L_\mathrm{p} = 17.3$ mm, $\mathrm{W_s} = 22.4$ mm, $L_\mathrm{s} = 32.9$ mm, $W_\mathrm{f} = 3.8$ mm, $L_\mathrm{f} = 15.6$ mm, and the height of the substrate $h = 1.57$ mm.

As the resonance phenomenon limits the antenna's bandwidth, a DSG was added to the conventional antenna's ground plan, as shown in Fig. 4, to achieve the wideband property. The introduction of a DGS alters the effective electrical length of the antenna, effectively introducing additional resonant modes and allowing for broader frequency coverage. The periodic patterns of the DGS create multiple resonances that collectively contribute to the wide-band response.

B. PARAMETRIC STUDY ON THE WIDE-BAND ANTENNA WITHOUT BAND NOTCHES

A few parameters were changed, and the accompanying results were recorded. This is to investigate the impact of various factors on the designed antenna's performance. The goal of parametric sweeping is to identify the parameters that influence the outcome and how they do so. Therefore, a parametric study must be carried out concerning all the identified critical characteristics to optimize the performance of the antenna. In this regard, a parametric sweep was performed on the patch Width *Wp*, the patch length *Lp*, and the antenna's partial ground plane length *Lg*. The impact of the gap width *G* between the ground plane and the patch was also verified. During the process, it was observed that a little variation in the substrate's length *Ls* and the width *Ws* was

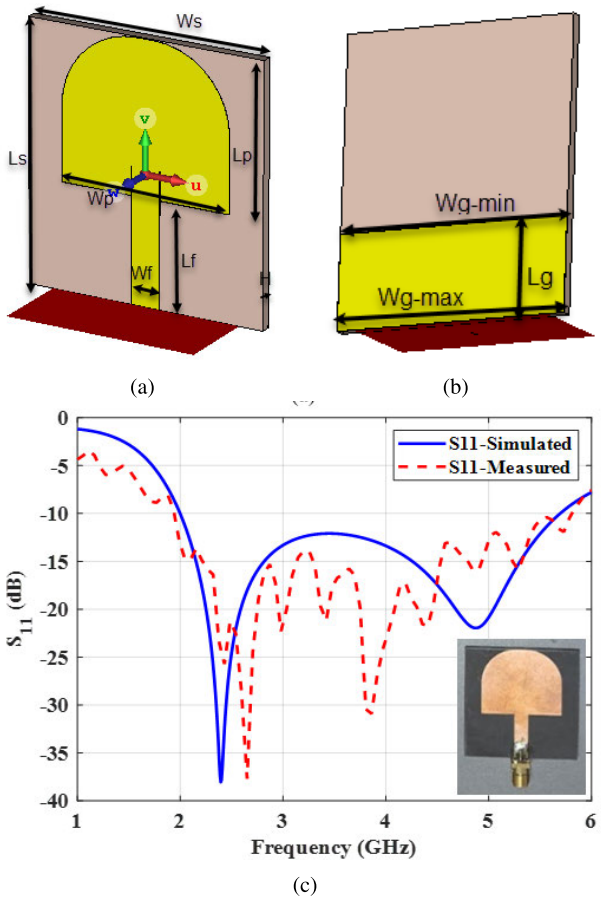

FIGURE 4. (a) Geometry of the antenna (top view), (b) geometry of the antenna (bottom view), (c) simulated and measured S_{11} for the wideband antenna with DGS.

observed and hence not provided because it had little impact on the antenna's performance.

According to Fig. 5(a), changing the value of L_p from 16 mm to 18 mm causes a change in the lower resonant frequency of the S_{11}. However, this fluctuation has minimal impact on the resonant frequency. Nevertheless, it does impact the magnitude of the S_{11}, which transitions from -35 dB to nearly -50 dB. Fig. 5(b) demonstrates that modifying the value of W_p enhances the antenna bandwidth by adjusting the higher resonant point, as perceived from the antenna's width perspective. It is important to mention that reducing the value of W_p from 20 mm to 18 mm causes a shift in the resonant point from 4.8 GHz to 5.4 GHz, resulting in an increased bandwidth on the higher frequency side. Fig. 5(c) demonstrates that increasing the ground plane width $W_{g_{\min}}$ from 10.7 mm to 18.73 mm results in a decrease in the return loss at the first resonant frequency and an increase in the bandwidth. Moreover, a rise in the minimum weight $W_{g_{\min}}$ causes a change of the higher resonant frequency in an upward direction. The modification in the value of $W_{g_{\min}}$ has an impact on both the bandwidth and the return loss.

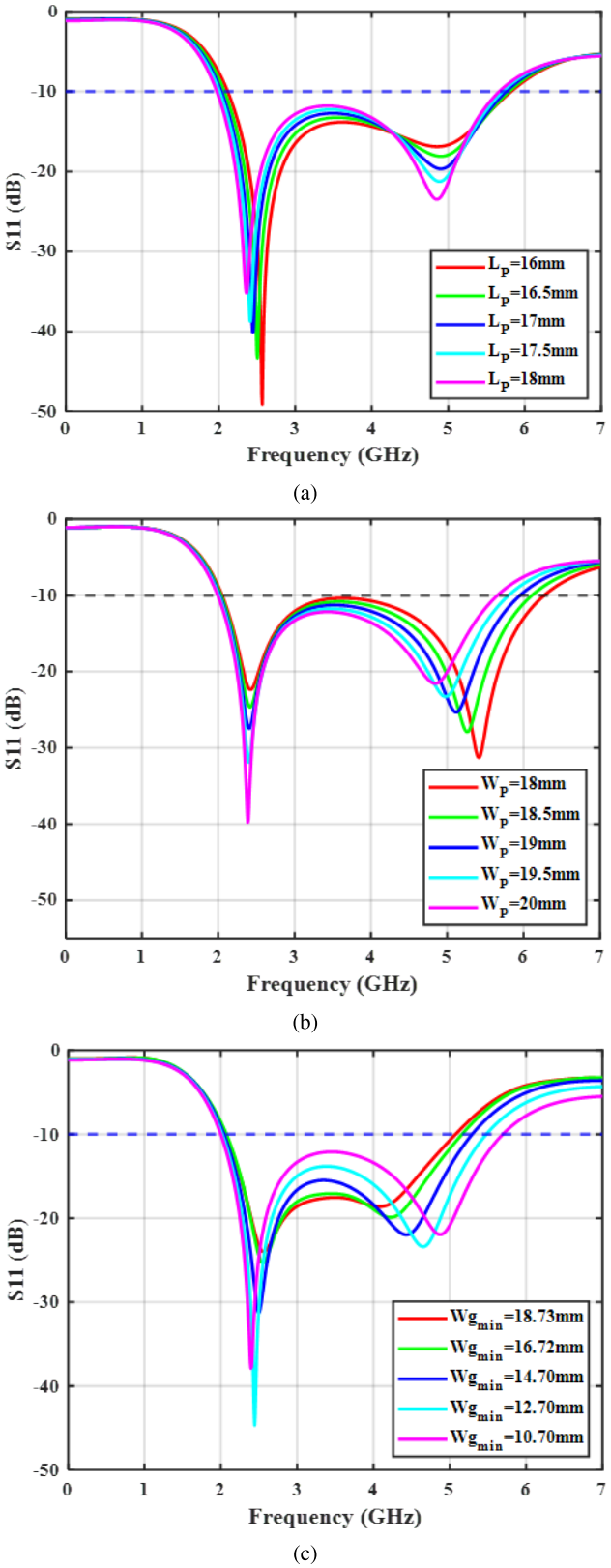

FIGURE 5. Parametric study of the widths of the wide-band antenna without band notches with changes in; (a) *Lp* (b) *Wp* (c) $Wg_{\min}$.

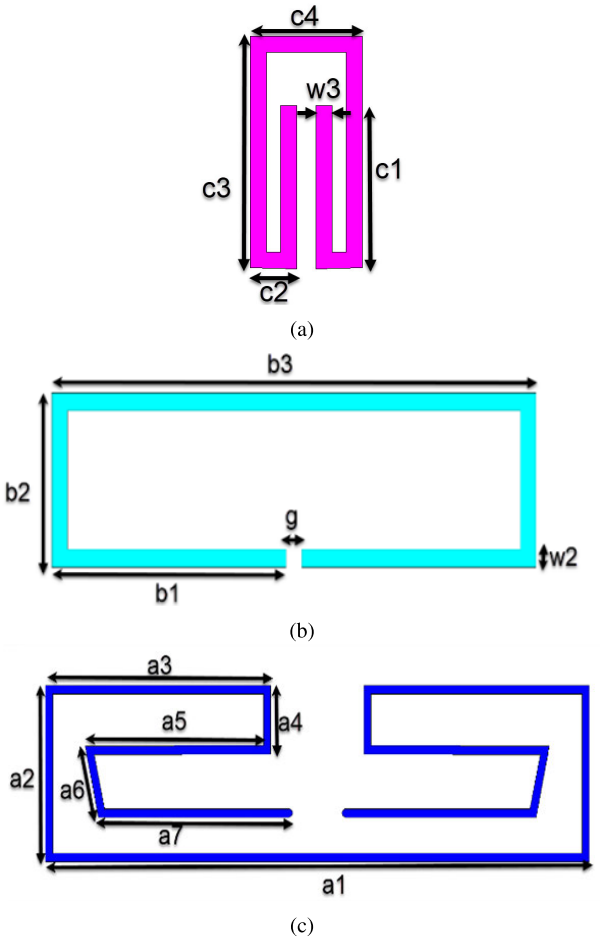

FIGURE 6. The structures of the three notches; (a) modified inverted U-slot, (b) a square ring slot, (c) interdigital inductor slot.

C. ANTENNA WITH THE TRI-BANDS NOTCH FILTERS

Establishing the operating bandwidth and the frequencies to be suppressed is the first step in designing the wide-band antenna with band notches capability. Reactive components were utilized as the band-notch mechanism. incorporating the band-notch mechanism into the antenna design and fine-tuning its specifications to provide the appropriate attenuation levels and notch frequencies. It was previously reported in [24] that slots with various shapes, including rectangular, circular, elliptical, or others, can be etched onto the patch to create notched bands. Nevertheless, conducting a full-wave electromagnetic simulation revealed that a slot with a shape similar to the patch antenna typically generates a stronger resonance compared to dissimilar shapes. This phenomenon arises from the concentration of current distribution along the patch's edges, which follows the same shape as the patch antenna.

Furthermore, it was discovered that the slot length plays a key role in influencing the notched frequency, in accordance with the empirical connection provided as follows [38].

$$f_{\text{notch}} = \frac{c}{2L\sqrt{\varepsilon_{\text{eff}}}} \tag{6}$$

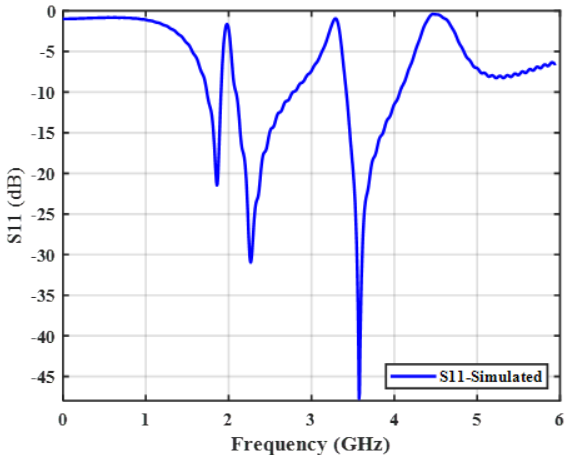

FIGURE 7. S_{11} of the tri-band notch antenna.

where the variables " ε_{eff} " and "c" corresponds to the approximate effective dielectric constant of the material and the free space speed of light respectively, with L denoting the overall length of the notch-shaped slot. It is vital to remember that the notched bandwidth can be somewhat modified by adjusting the width of the slot, whereas the length is responsible for a shift in the resonant frequency. Consequently, by fine-tuning the slot length and width, a specific notched frequency band can be achieved.

Fig. 6 shows the shapes of the three notches along with their dimensions where: $a_1 = 15.16\text{mm}, a_2 = 3.60\text{mm}, a_3 = 5.53\text{mm}, a_4 = 1.50\text{mm}, a_5 = 4.45\text{mm}, a_6 = 1.60\text{mm}, a_7 = 4.65\text{mm}, b_1 = 6.74\text{mm}, b_2 = 3.65\text{mm}, b_3 = 13.97\text{mm}, w_2 = 0.5\text{mm}, G = 0.5\text{mm}, c_1 = 3.90\text{mm}, c_2 = 1.30\text{mm}, c_3 = 5.83\text{mm}, c_4 = 2.92\text{mm}, w_3 = 0.5\text{mm}$.

To generate a band-notched feature, several slots were etched onto the top of the wideband (WB) antenna patch in accordance with the technique illustrated in references [24]. These etched slots are designed to resonate at specific frequencies according to equation is referring to equation (6), effectively providing band-notched features in the antenna's performance.

To create these notches, three different slots were etched onto the patch: one was shaped like a modified inverted U-slot, while the other two were shaped like a square ring and interdigital inductor slots. Together, these slots produced the triple triple-notched bands. The square ring resonator creates the middle-band notch at 3.2 GHz, the modified inverted U-slot creates the higher band notch at 4.5 GHz, and the inductor induces the lower notch frequency at 2.0 GHz. The three resonant bands from the WB antenna 1.9 GHz, 2.4 GHz, and 3.5 GHz are the result of these notches. The tri-band notch antenna's S_{11} is plotted against frequency as shown in Fig. 7.

D. EFFECTS OF THE NOTCH PARAMETERS ON ANTENNA PERFORMANCES

A computer simulation was used to evaluate the triple-band notched antenna through a parametric investigation. The

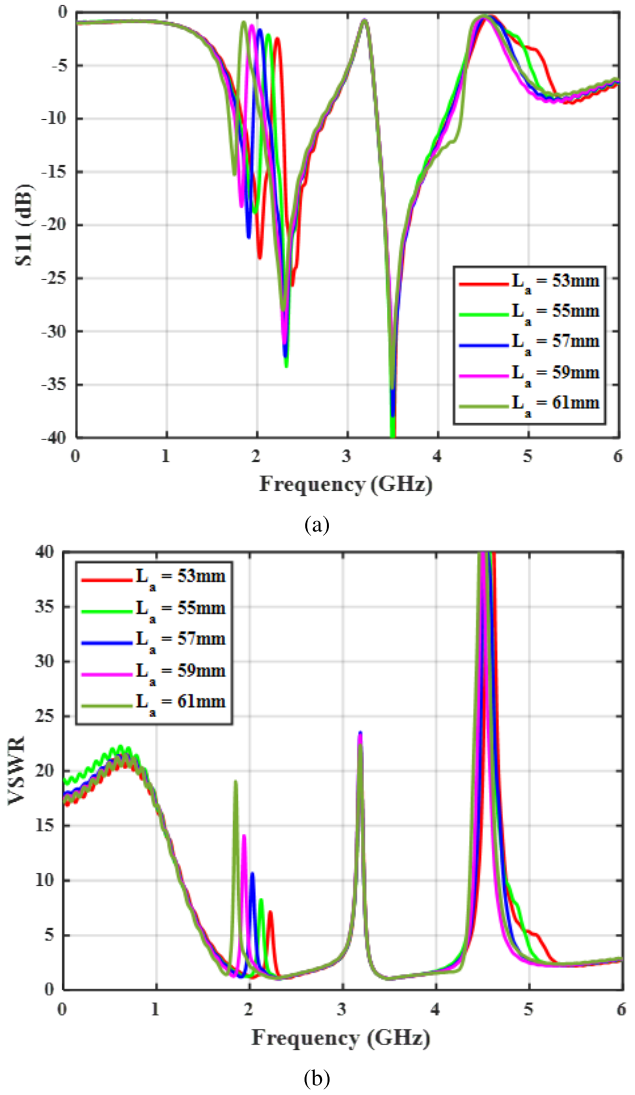

FIGURE 8. Effect in variation of length of the interdigital inductor slot on; (a) the S_{11}, (b) the VSWR.

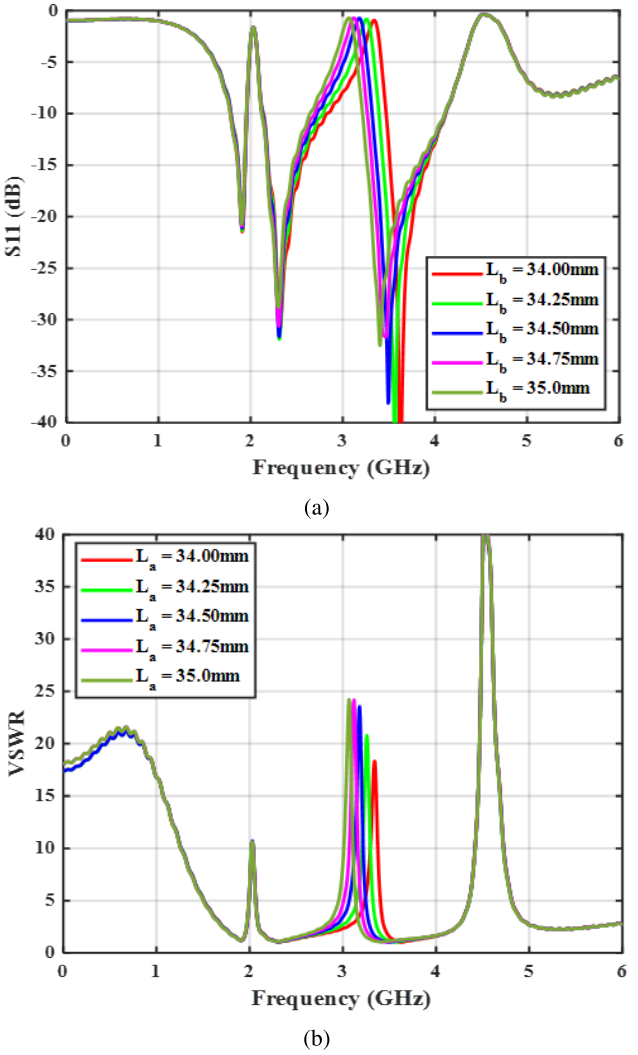

FIGURE 9. Effect in variation of length of the square ring resonator on; (a) the S_{11}, (b) the VSWR.

study aimed to comprehend the influence of the length of individual resonant components on the effectiveness of band notches. Specifically, the inductance is influenced by the length and width of each resonator, whereas the capacitance is governed by the distance between neighboring arms.

As discussed in references [28], the interactions between the resonators and the primary radiator function as a filtering mechanism, resulting in the production of a notch band at a given frequency. Fig. 8 illustrates the relationship between the lengths of different resonant parts and their effects on both the band notch characteristics and the Voltage Standing Wave Ratio (VSWR) of the triband antenna.

From this figure, it is obvious that changing the inter-digital inductor slot's length has an impact only on the lower frequency notch, while the intermediate and higher notch frequencies remain untouched. When this length was modified within the range of 53 mm to 61 mm, encompassing the optimal length of 57.82 mm for the notch, the outcome was a change in the positions of the notch frequencies, shifting from 1.85 GHz to 2.22 GHz. The values of notching were −0.95 dB at 1.85 GHz and −2.61 dB at 2.22 GHz.

On the other hand, altering the square ring resonator's length changed the notch frequency at 3.2 GHz but did not affect the two outermost notch frequencies. As illustrated in Fig. 9, adjusting the notch frequency length (L_b) within the range of 34 mm to 35 mm led to a shift in the notch frequency from 3.01 GHz to 3.28 GHz, accompanied by notch levels of −0.61 dB and −0.84 dB, respectively.

For the modified inverted U-slot, it is evident that its notch occurs at a frequency of 3.2 GHz. When its length was varied from 24 *mm* to 25 *mm*, the corresponding notch frequency shifted as shown in Fig. 10. However, this variation does not affect other notch frequencies. When the length was reduced to 24 *mm*, the frequency shifted up to 4.73 GHz with an attenuation level of −0.45 *dB*. Also, when the notch length was increased to 24 *mm*, the corresponding frequency shifted down to 4.33 GHz with an attenuation at −0.37 *dB*. In all

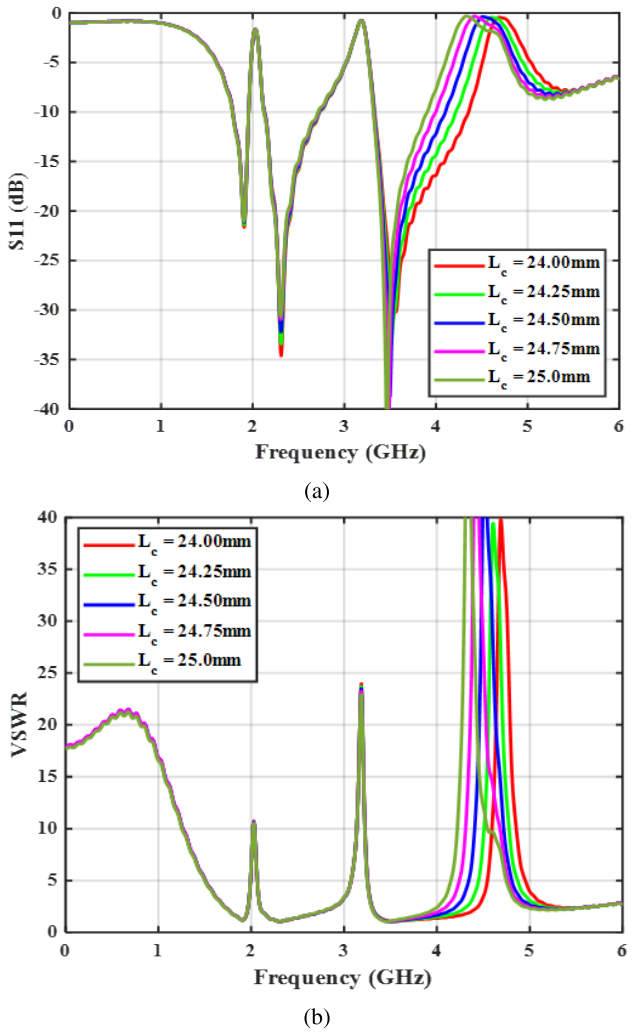

FIGURE 10. Effect in variation of length of the modified inverted U-slot on; (a) the S_{11}, (b) the VSWR.

cases, it is worth noting that, a downward shift in the notching frequency improved the noting level whereas, the notching level decreased as the frequency increased.

Fig. 11 presents the layout, simulated and measured S_{11}, and the VSWR of the proposed triple-band notch antenna. The S_{11} clearly shows the three resonance frequencies at 1.9 GHz, 2.3 GHz and 3.5 GHz, with the lowest value of -18.79 dB at 1.9 GHz and the highest value better than -40 dB occurring at 3.5 GHz. However, the level of the notching at the three different notch frequencies is -1.76 dB, -1.47 dB, and -0.4 dB respectively as seen in Fig. 11(b). These notching levels correspond to the depth of the notch formed in the S_{11} curve at the resonant frequency, which indicates the maximum attenuation (in dB) of the reflected signal, occurring at the notch frequencies. Both the simulated and the measured results agreed with little disparity which could be due to measurement imperfection and cable losses. This indicates the effectiveness of the tri-band antenna in rejecting frequencies that are not desired.

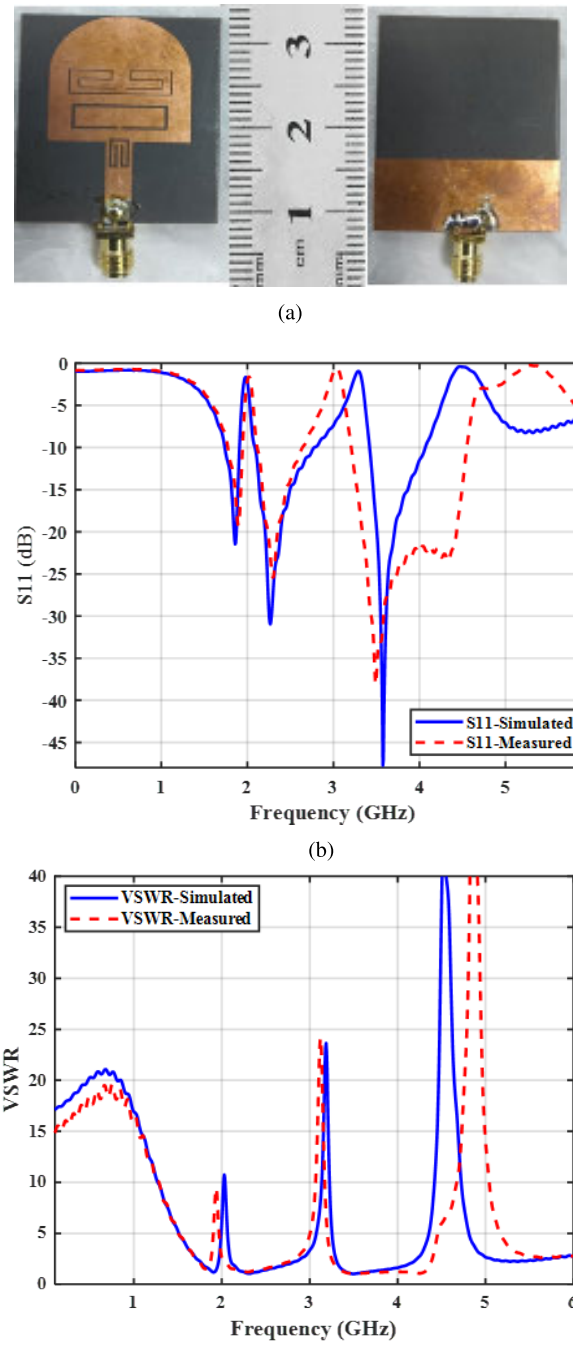

FIGURE 11. The tri-band notch antenna. (a) Photograph of the prototype, (b) the S_{11} (c) the VSWR.

From the simulated VSWR against frequency for the band-notch antenna shown in Fig. 11(c), It is seen that the proposed antenna exhibits the three notched bands at the desired frequencies while maintaining a wideband performance for VSWR $<$ 2, covering the entire frequency bands. Except for the point at 4 GHz, where the measured result deviates slightly from the predicted VSWR, it could be observed that the results obtained experimentally, and the simulated ones coincide extremely well. Additionally, the

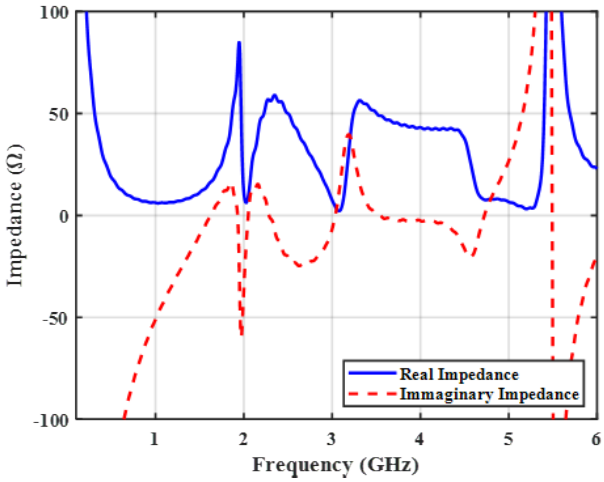

FIGURE 12. Real and imaginary impedance curve of the tri-band notch.

designed antenna covers the complete WB frequency band with triple notched bands and has a consistent performance with a VSWR $<$ 2 at 1.9 GHz, 2.3 GHz, and 3.5 GHz. The measured VSWR is significantly greater than 2 in the three desirable notched bands.

IV. ADS EQUIVALENT CIRCUIT MODEL ANALYSIS

The impedance curve of the wideband antenna with the three notches is shown in Fig. 12. For this band notch antenna, a close look at the curve revealed an approximate value of the real impedance to be around 50 -ohms at the resonant frequencies; 2.0 GHz, 3.6 GHz, and 4.5 GHz. At these frequencies, the imaginary part of the impedance has positive slopes indicating a series resonance at the notch frequencies.

However, to obtain the equivalent parallel RLC equivalent circuit representing the band-notch antenna, the radiation resistance, R and the two resonant elements L and C representing the antenna model need to be found either by analytic means or by using the results obtained from any 3D Full-wave EM-Field Solver for High-frequency such as ANSYS 3D high-frequency simulation software (HFSS) or computer simulation system (CST).

From the Impedance curve presented in Fig. 12, several peaks and valleys can be observed from the plot which represent different impedances. The impedances representing the proposed antenna are obtained at the three resonance frequencies. For calculating the corresponding values for the inductors and the capacitors at the resonance frequencies, equations were used along with the impedance curve from CST studio suit obtained from the impedance curve, and the values were summarized in Table 1.

For the first resonance frequencies at 1.9 GHz the approximate curve impedance which represents the radiation resistance is 58.7 Ω, the corresponding capacitance and inductance are 0.1132 pF and 6.198 pH respectively. Similarly, the RLC values at 2.3 GHz are approximately

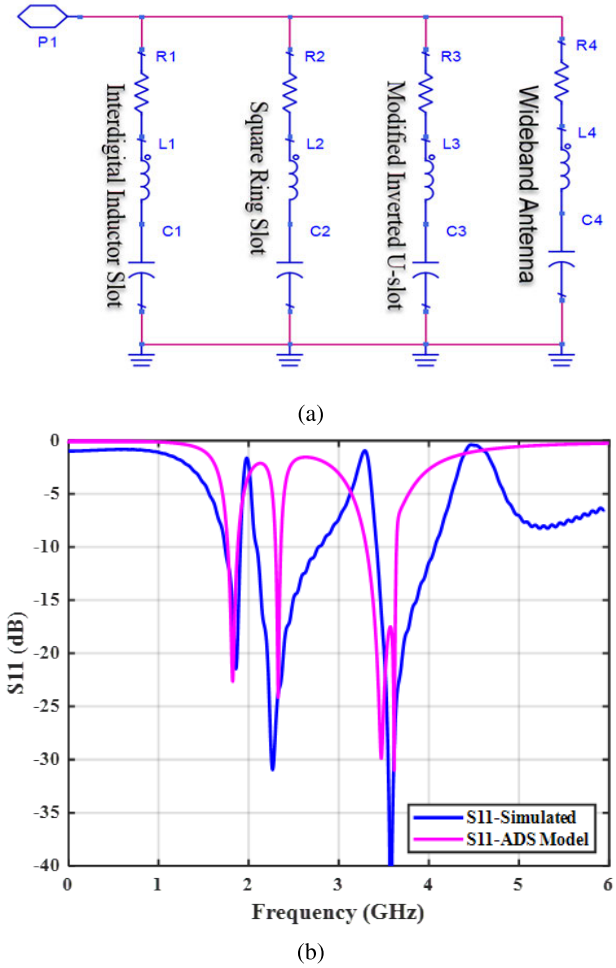

FIGURE 13. The tri-band notch antenna (a) ADS circuit model (b) the S_{11} comparison.

TABLE 1. Lumped elements Values for the RLC equivalent circuit.

Freq. (GHz)	$\mathbf{Z_{11}(\Omega)}$	$\mathbf{Im\,(Z_{11})\,(\Omega)}$	$\mathbf{L(pH)}$	$\mathbf{C(pF)}$
1.90	58.7	7.4	6.1979	0.1132
2.00	6.4	18.42	1.4656	4.3196
2.30	56	1.3	0.0899	0.5322
3.00	2.89	4.83	0.2562	0.1098
3.50	50.09	0.3	0.0136	0.0152
4.50	15.27	16.57	0.5860	2.1300

56 Ω, 0.0899 pH and 0.5322 pF respectively. At 3.5 GHz, the radiation resistance is 50.1 Ω, and the inductor and capacitor are 0.0136 pH and 0.0152 pF respectively. This set of parameters was used as the initial parameter to obtain the ADS equivalent circuit model of the triband antenna, and the optimized model along with the S_{11} plot are shown in Fig. 13.

V. ANTENNA SURFACE CURRENT DISTRIBUTION

Surface current distribution refers to how electric current is distributed across the antenna's surface. It is a crucial parameter in antenna design since it has a significant impact on the radiation pattern, impedance, and gain. By strategically placing notches in the antenna design, it can be made to operate efficiently in multiple frequency bands, this allows

the antenna to transmit or receive signals on the desired frequency bands while minimizing interference and radiation in unwanted frequency ranges. The proposed monopole antenna having three notches was designed to resonate at 1.9 GHz, 2.3 GHz, and 3.5 GHz. It has a surface current distribution that is different from the wideband monopole antenna presented without notches. In the case of the notch- antenna, at every notch frequency, the surface current distribution is disrupted, resulting in a reduction in radiation at those frequencies and hence suppressing radiation at that frequency.

Fig. 14 shows the normalized surface current distribution for the tri-band notch antenna at each of the three notch frequencies. From this figure, it can be observed that all radiation is blocked around the notch frequencies, and hence the notched bands are formed. Examining current distributions at the notch frequencies, where the current density is more evident near the notch geometry, also clearly explains this behavior. The current directions in identical arms of resonant elements are in opposite directions, resulting in mutual cancellation. Consequently, the antenna fails to transmit at that specific frequency, resulting in the emergence of a frequency notch at that particular position. Fig. 14(a) illustrates the distribution of surface current on the antenna at a frequency of 2.0 GHz, specifically in the region where radiation is reduced. This can be seen from the intensity scale of the current distribution and the VSWR curve depicted in the same figure. The value of the VSWR at that frequency falls above the threshold of 2. Similarly, at the notch frequencies of 3.2 GHz, the intensity is high at the vicinity where the notch is located, which results in radiation null at the notch frequency as shown according to the ramp color of Fig. 14 (b). A similar sicario occurred for the third notch frequency where there are more current distributions near the third notch occurring at the notch-band frequency of 4.5 GHz as illustrated in Fig. 14 (c). The red hue on the intensity scale consistently indicates the maximum current density in all circumstances.

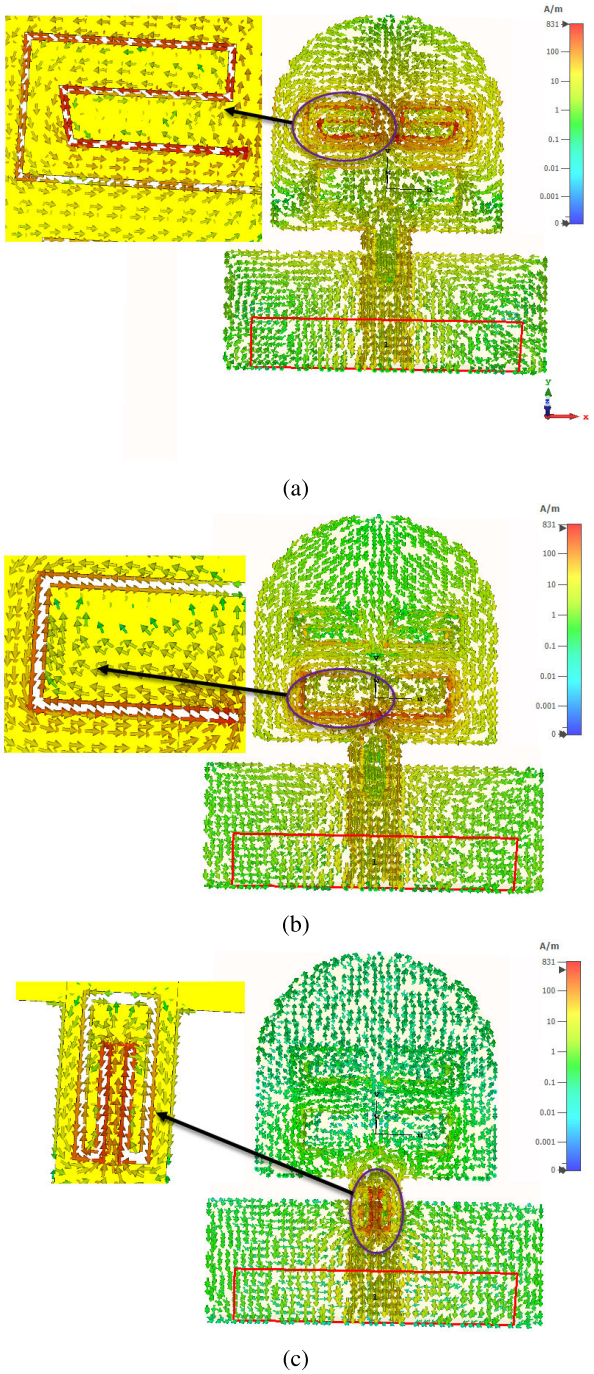

FIGURE 14. Surface current distribution of the tri-band notch antenna at; (a) 2.0 GHz, (b) 3.2 GHz, (c) 4.5 GHz.

VI. GAIN, EFFICIENCY, AND RADIATION PATTERN

In most applications, WB antennas require an omnidirectional pattern in the plane perpendicular to the radiating patch. The proposed tri-band antenna was constructed with radiation nulls at 2.0, 3.2, and 4.5 GHz, yielding a suitable radiation pattern at 1.9, 2.3, and 3.5 GHz. Fig. 15 shows an image of the antenna being tested, while the normalized co/cross radiation patterns in the E-plane at frequencies of 1.9, 2.3, and 3.5 GHz are respectively displayed in Fig. 16(a)–(c). The plot demonstrates that the copolarized fields of the radiation patterns are omnidirectional across all frequencies inside the passband. However, two nulls in the cross-polarization fields were seen at all resonant frequencies, which are identical to those observed in conventional monopole antennas. While higher-order harmonics can sometimes be the cause of nulls at higher frequencies, the antenna maintains a consistent and uniform radiation pattern across its entire operational range. Manufacturing tolerance and discrepancies between the reference and test antennas might result in irregularities in the radiation patterns, causing ripples. The power loss of the RF wire during the experiment may have contributed to the generation of some of these waves.

The realized gain of the proposed tri-band notch antenna is illustrated in Fig. 17. At a frequency of 1.9 GHz, the antenna gain is roughly 0.89 dBi, which is extremely near to the gain of an ideal omnidirectional antenna. As frequency rises, the

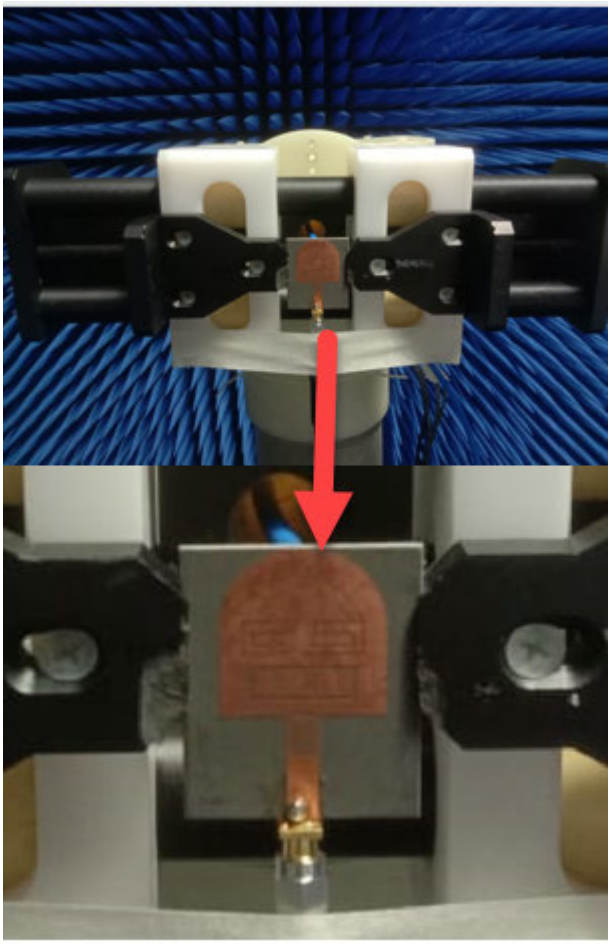

FIGURE 15. Photograph of the device under test.

gain nudges up, and a peak gain of 4.7 dBi is measured. At the notch frequencies of 2 GHz, 3.2 GHz and 4.5 GHz, the gain quickly fell after achieving peak value at the resonant frequencies just before the notches. It's vital to note that there are large gain decreases that may be identified immediately after the three notch bands are verified that the proposed antenna is suppressing the signal efficiently near notch bands.

Apart from other characteristics, such as the antenna's radiation pattern, impedance, and gain, the efficiency of an antenna is another significant element to be considered when selecting an antenna for a certain application. As depicted in Fig. 18, the efficiency plot of the proposed triband antenna includes three resonance frequencies: 1.9 GHz, 2.3 GHz, and 3.5 GHz. From the plot, it can be noticed that it exhibited a clear efficiency peak at these resonant frequencies, indicating strong radiation efficiency and impedance matching at those frequencies, with the highest efficiency of 95.4% at 4.2 GHz. Between these peaks are regions of relatively high efficiency, demonstrating the antenna's effective operation within the frequency bands containing these resonant points. Efficiency valleys formed outside these ranges, indicating lower radiation efficiency due to impedance mismatches.

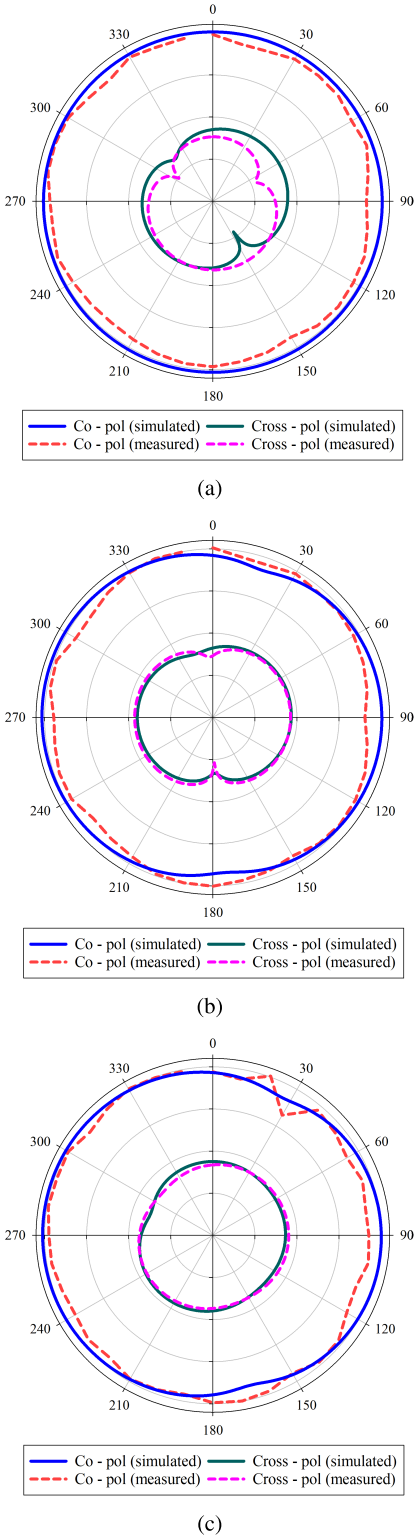

FIGURE 16. Simulated and measured co and cross polarization polarization patterns of the tri-band notch antenna at. (a) 1.9 GHz, (b) 2.3 GHz, (c) 3.5 GHz.

These minimum gains can effectively minimize external interferences. The plot's overall shape consists of a series of peaks and valleys, demonstrating the antenna's capacity

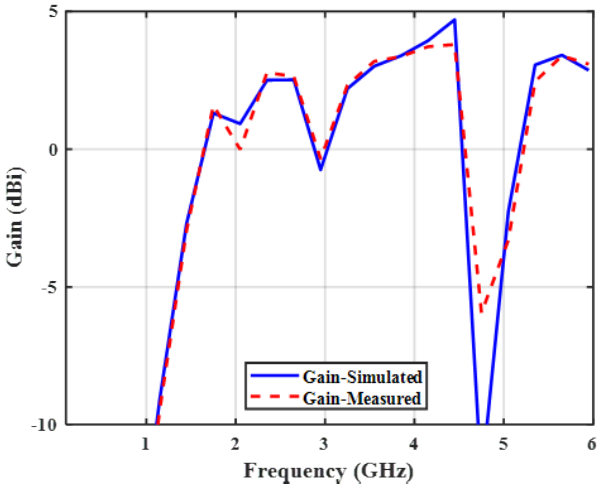

FIGURE 17. Gain of the tri-band notch antenna.

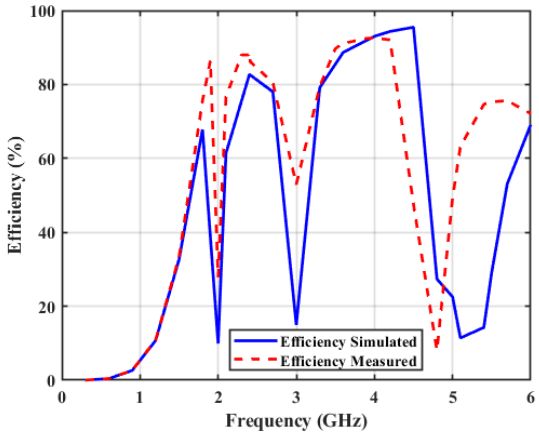

FIGURE 18. Efficiency of the tri-band notch antenna.

to work efficiently in the desired frequency ranges while suppressing interference at the notch frequencies, making it well-suited for multi-band applications.

VII. MACHINE LEARNING (ML) BASED OPTIMIZATION

In this section, Machine Learning (ML) techniques are explored for predicting all the frequency points along the S_{11} curve of the proposed triband antenna designed. These predictions were compared against the simulated results obtained using the antenna modeling technique. Designing, analyzing, and enhancing electromagnetic (EM) components and systems involves the use of numerical analysis techniques including the Finite Element Method (FEM), Methods of Moments (MoM), and Finite Difference Time Domain (FDTD). These methodologies are often applied with 3D EM simulators like ADS, HFSS, and CST programs [41]. However, the more sophisticated the antenna design is, the longer it takes for software like CST and HFSS to complete the optimization process. This limitation has an impact on optimization methods that are now in use, which are essential for ensuring a quicker design process for a strong antenna

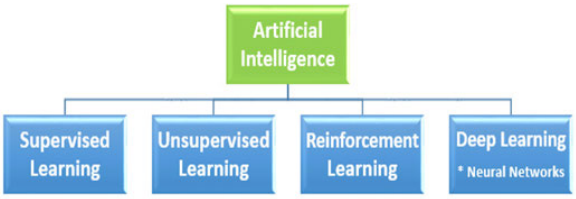

FIGURE 19. Machine learning models [43].

that emits at maximum capacity. Scientists are studying ways to utilize machine learning (ML) and deep learning (DL) algorithms to increase antenna design processes [42]. This is because these techniques may dramatically speed up design while maintaining high accuracy, they hold immense promise for boosting design and anticipating antenna behavior. Both ML and DL are families of artificial intelligence as depicted in Fig. 19.

From the general ML model shown in Fig. 19 and the type of input/output data sets, supervised learning was used for the prediction. The flow chart detailing the procedure is shown in Fig. 20. Since the problem is parametric and nonlinear, the optimization problem was solved using a parametric nonlinear model that depicts the relationship between the response variable and predictor [44]. It is generally expressed as follows:

$$y = f(x, \beta) + \varepsilon \tag{7}$$

where

- The response variable's observations are represented by the n-by-1 vector y.
- A function f is any function of X and β that calculates the prediction for the corresponding row of y by evaluating each row of x and the vector β.
- x is a predictor matrix consisting of n by p rows, one column for each predictor, and one row for each observation.
- β is a vector with p by 1 unknown parameter that needs to be calculated.
- An n-by-1 vector of independent random disturbances with identical distributions is represented by ε.

In this paper, the prediction of antenna gain and efficiency was formulated as an optimization problem. After that, the raw data was extracted from the CST studio suit. the data was cleaned to ensure it was free from outliers. It was further divided into training and test portions thereafter. several machine learning algorithms were utilized to solve this problem. The goal of the optimization problem is to learn the mapping of the inputs to predict the outputs (antenna gain and efficiency) such that the error between the predicted and the actual value will be minimal. The mathematical model of this optimization problem is to minimize the function in (8) [45]:

$$\min_{f}(y, f(x, \beta)) \tag{8}$$

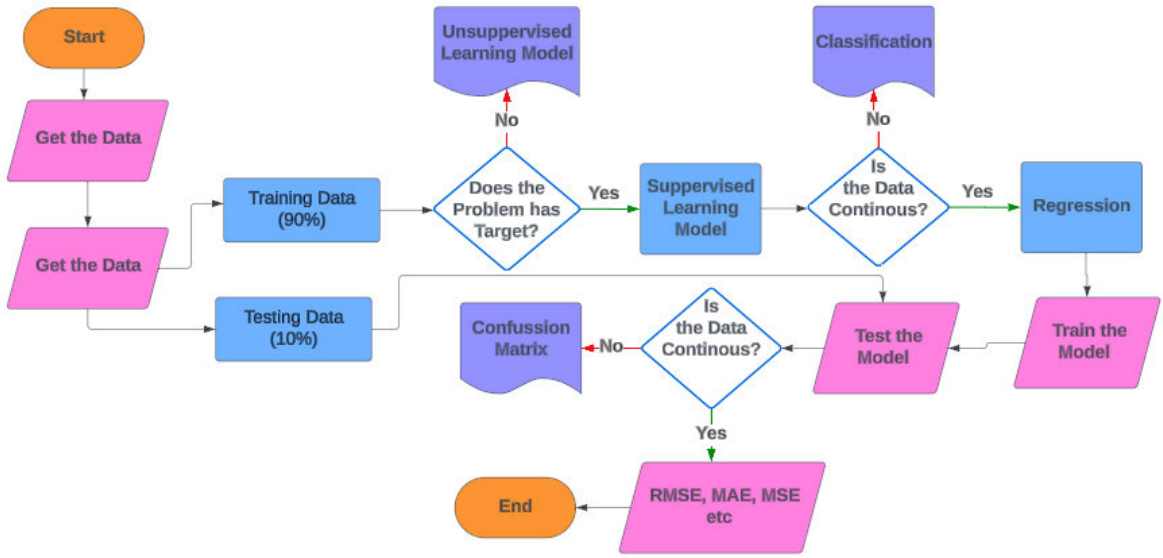

FIGURE 20. Implementation machine learning workflow.

A. SELECTION OF THE DATA SETS AND THE ALGORITHM

For any prediction to be ensured, there must be some sets of input/output data to feed the system. In this research, the antenna was designed using the model provided in [40] and the physical parameters of the antenna were modeled in CST studio. Trust region framework and Genetic algorithm were used to optimize the antenna in the CST environment. Having run several optimizations taking the variables described in Sections III-A and IV as the input and for each optimization run, the corresponding outputs were taken and recorded. In total, 7007 sets of inputs and outputs were used for the S11 prediction. The available data was reshuffled and divided into 90% for training, and the remaining 10% was reserved for validation. A fresh data equivalent to 10% was obtained and used for the testing. The idea of using separate data for the testing is to substantiate the robustness of the model.

There are many algorithms utilized by researchers for ML prediction. Among these algorithms are Linear Regression, Decision Trees, Support Vector Machines (SVM), Gaussian Process Regression, Ensemble, and so on. Each has its strengths and weaknesses. The choice of any algorithm depends on the researcher and the nature of the problem. In this research, the following algorisms algorithms were explored.

1) LINEAR REGRESSION (LR)

Linear regression is a fundamental tool in data analysis due to its simplicity and ease of comprehension. However, its usefulness in complex datasets could be restricted by its assumption of a linear correlation between variables. Nevertheless, it remains a valuable instrument for trend analysis and prediction in well-organized data [46].

2) EFFICIENT LINEAR REGRESSION (ELR)

The purpose of efficient linear regression is to maximize the predictive performance of the linear regression (LR) model without sacrificing its processing efficiency. This is performed using a variety of ways and methods. A typical statistical method for simulating the relationship between a dependent variable and one or more independent variables is linear regression. However, typical procedures could become computationally expensive or even impractical for enormous datasets or high-dimensional scenarios. These obstacles are met by successful linear regression algorithms, which make take advantage of algorithmic improvements, computational short cuts, or optimization methodologies [47].

3) DECISION TREES REGRESSION (DTR)

Non-parametric supervised learning methods, such as decision trees, are utilized for regression and classification tasks. The feature space is divided iteratively based on input variable values to reduce impurity or increase information gain at each division. Decision trees are flexible and able to handle data with non-linear correlations. However, they are susceptible to overfitting, especially in situations involving complex and detailed trees [48].

4) SUPPORT VECTOR MACHINES REGRESSION (SVMR)

Strong supervised learning models for classification and regression applications include Support Vector Machines (SVM). SVM aims to optimize the margin between classes or fit the data with the least amount of error by identifying the optimum hyperplane to partition classes or fit the regression line. SVMs operate well with high-dimensional data and are noise-resistant. But they can be computationally expensive, especially when dealing with enormous

datasets, and hence demand careful attention when choosing hyperparameters [49].

5) GAUSSIAN PROCESS REGRESSION (GPR)

A non-parametric Bayesian approach to regression, Gaussian Process Regression models function distributions as opposed to point estimations. In addition to projections, it delivers estimates of uncertainty and can respond to intricate data patterns. But Gaussian Process When a dataset expands in size, regression can become computationally demanding [50].

6) KERNEL APPROXIMATION REGRESSION (KAR)

Kernel methods are a class of algorithms that operate by implicitly mapping input data into high-dimensional feature spaces, where linear relationships become apparent. They are particularly suitable for high-dimensional data and can adapt to various data patterns through different kernel functions, such as polynomial kernels and Gaussian kernels [51].

7) ENSEMBLE TREE REGRESSION (ETR)

Ensemble methods combine multiple base models to improve predictive performance. They are less prone to overfitting and instability compared to individual models. Random Forest and Boosted Trees are popular ensemble techniques used for regression tasks, leveraging the strengths of multiple models to achieve better generalization [52].

B. PERFORMANCES METRICS

To assess a model's performance, many measures are applied. They generally offer perceptions regarding the correctness and trustworthiness of forecasts. Mean Squared Error (MSE), Mean Absolute Error (MAE), Root Mean Squared Logarithmic Error (RMSLE), Mean Squared Logarithmic Error (MSLE), Mean Absolute Percentage Error (MAPE), and the variance score (R-squared) are the metrics that are often applied.

1) MEAN ABSOLUTE ERROR

The average absolute difference between the expected and actual values is assessed by the Mean Absolute Error, or MAE. Better accuracy is demonstrated by a lower MAE, where each inaccuracy contributes the same amount to the total measure. It is less vulnerable to outliers than MSE, though. The Expression of MAE Mathematically as [53]:

$$MAE = \frac{1}{n}\sum_{i=1}^{n}\left|y_i - \hat{y}_i\right| \tag{9}$$

where n denotes the number of observations, y_i is the actual value, and $\hat{y}_i$ is the predicted value, and the difference $\left|y_i - \hat{y}_i\right|$ represents the absolute error.

2) MEAN SQUARED ERROR (MSE)

MSE is the average of squared discrepancies between anticipated and actual values. It penalizes greater errors more severely than MAE, creating a metric that is sensitive to outliers.

$$MSE = \frac{1}{n}\sum_{i=1}^{n}\left(y_i - \hat{y}_i\right)^2 \tag{10}$$

This is similar to MAE in equation (7) but errors are squared before averaging.

3) MEAN SQUARED LOGARITHMIC ERROR (MSLE)

MSLE measures the average of the logarithmic square differences between anticipated and actual values. It is appropriate for models where the relative variations between anticipated and actual values are more relevant than absolute differences. It is represented by:

$$MSLE = \frac{1}{n}\sum_{i=1}^{n}\left(\log\left(1 + y_i\right) + \log\left(1 + \hat{y}_i\right)\right)^2 \tag{11}$$

where n is the number of observations, y is the actual value, and $\hat{y}$ is the predicted value with log denotes denoting the natural logarithm.

4) ROOT MEAN SQUARED LOGARITHMIC ERROR (RMSLE)

RMSLE is the square root of MSLE, providing an error measure in the same scale as the target variable. It is very useful for evaluating the performance of models on datasets with varying scales.

$$\text{RMSLE} = \sqrt{\frac{1}{n}\sum_{i=1}^{n}\left(\log\left(x_i + 1\right) - \log\left(y_i + 1\right)\right)^2} \tag{12}$$

5) MEAN ABSOLUTE PERCENTAGE ERROR (MAPE)

Mean Absolute Percentage Error expresses errors as a percentage of actual values, taking into account relative disparities. It is especially useful for presenting a model's accuracy in percentage error, which makes it easier to interpret.

$$\text{MAPE} = \frac{1}{n}\sum_{i=1}^{n}\left|\frac{y_i - \hat{y}_i}{y_i}\right| \times 100\% \tag{13}$$

These metrics are often used for assessing the performance of regression models, providing information about the accuracy and dependability of predictions. It is critical to select the most appropriate metric depending on the problem's specific characteristics and requirements.

VIII. MACHINE LEARNING PREDICTION RESULTS

Several runs were carried out with the aim of choosing the best algorithm for the prediction according to the available data. This step is necessary as it was reported that there is no better algorithm than the others. Rather, an algorithm depends on the nature of the problem intended to be solved.

Table 2 depicts the result comparing the performance among the chosen algorithms. From these results, Gaussian Process Regression was found to be the best option for the data sets. It was chosen because it displayed the lowest error

TABLE 2. Performance parameters of all the algorithms with the same architecture.

Algorithms	MAE (%)	MSE (%)	MSLE (%)	RMSLE (%)	MAPE (%)	RMSE (%)	Vscore%
Gaussian Process Regression	0.7163	2.3623	0.0554	0.4008	9.1272	1.5370	97.3624
Ensemble Regression	0.7910	2.9114	0.1283	0.3613	10.3532	1.7063	96.7494
SVM Regression	0.9060	3.5584	0.0567	0.3355	11.0544	1.8864	96.0269
Decision Tree Regression	1.1987	3.8707	0.6354	0.8598	12.3040	1.9674	95.6783
Kernel Regression	5.1241	7.6528	1.2324	1.3251	23.2340	7.3191	40.1882
Efficient Linear Regression	7.3169	12.1695	3.8045	2.3044	36.7055	9.2297	4.8869

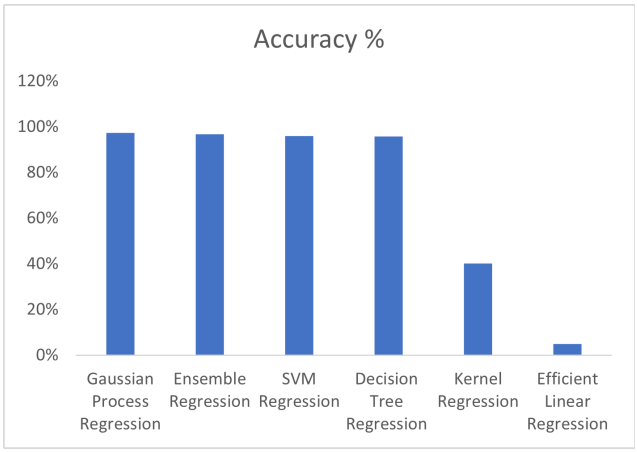

(a)

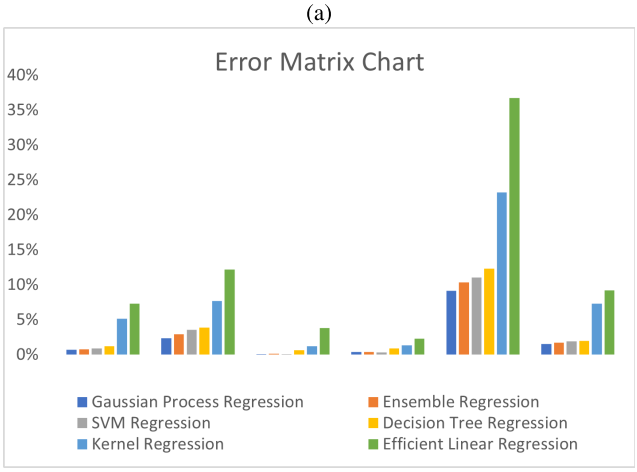

(b)

FIGURE 21. Performance parameters of the six algorithms; (a) the accuracy chart, (b) the error chart.

in terms of MAE, MSE, MSLE, RMSLE, MAPE, and RMSE. It however has the highest accuracy in terms of V-score and R-square, which stands at 97.36%.

From this error matrix chart, it can be observed that the Gaussian process regression exhibited the lowest error of 0.0554% from all the performance matrices. The ensemble regression was the second best followed by the SVM and the kernel regression. The maximum error of 36.7% was recorded from the linear regression, which ranked it the worst, followed by the decision tree regression. the reason for LR being the worst is attributed to the fact that it is specifically designed for sets of data where there exists a linear relationship between the input and the output quantities. This can be seen from the accuracy values of 4.88% recorded and displayed in Table 2 and Fig. 21.

After choosing the Gaussian Process Regression as the best algorithm according to the results displayed in Table 2 and the accuracy chart depicted in Fig. 21, several iterations were repeatedly run, validated, and tested. In each case, the performances of the runs are recorded in terms of MAE, MSE, MSLE, RMSLE, MAPE, and RMSE. From this result, the best of the algorithms was chosen for the prediction of S_{11} and the radiation efficiency. Fig. 21 shows the predicted S_{11} along with the actual simulated value. From the predicted curve, it can be seen that the GPR predicted the S_{11} smoother than the rest, followed by ER. the next best predicted S_{11} are the SVM, DTR, and the KR. However, when new sets of inputs were supplied into the linear regression model, it could not predict a replica of the outputs as predicted by other models. The ELR is therefore regarded as the worst-performing model among all the algorithms. the reason behind the worse performance of the ELR is that it was formulated to efficiently work when there is a linear relationship between the inputs and the outputs, which is not the case with the data extracted from the CST studio. It is worth noting that the Kernel algorithm is the second worst in terms of prediction. Compared with the other models, it was not able to predict the first notch accurately. Table 3 shows a comparison between the predicted and the actual S_{11} obtained from the best-predicted algorithm. This can also be seen from the graphs displayed in Fig. 22. It can be noted that the ensemble regression was able to predict the output very accurately as compared to the GR, but the output curve was not very smooth when compared to the GR. The results presented in both Fig. 22 and Table 2 are in order from the lowest error to the highest.

For the predicted efficiency, all the models presented in Fig. 23 show a good prediction. A close look at the curves clearly shows a very good prediction at the lower frequencies up to 4.89 GHz for all the models presented. Immediately after this frequency, the prediction deteriorates. However, the GPR is better than the rest as it has the lowest error and exhibits the highest accuracy.

By feeding in variables like length, width, substrate specifications, and other notch filter characteristics, this model may be used to approximate the S_{11} and efficiency of the proposed triband antenna and produce the associated outputs. It removes the requirement to

TABLE 3. Comparison of the Simulated and the predicted S_{11}.

S/N	SIMULATED S11 (dB)	PREDICTED S11 (dB)	Error	S/N	SIMULATED S11 (dB)	PREDICTED S11 (dB)	Error	S/N	SIMULATED S11 (dB)	PREDICTED S11 (dB)	Error
1	-12.9272	-13.4632	0.5360	16	-13.8570	-14.3574	0.5004	31	-5.4363	-5.4010	-0.0353
2	-18.1994	-19.1083	0.9089	17	-5.2717	-5.5909	0.3192	32	-4.2387	-5.0105	0.7717
3	-11.4533	-11.6482	0.1949	18	-26.0299	-24.4438	-1.5861	33	-9.5892	-6.3544	-3.2348
4	-0.3089	-0.3879	0.0790	19	-0.9842	-0.9388	-0.0454	34	-1.2743	-1.2268	-0.0475
5	-0.9793	-0.9388	-0.0406	20	-6.1855	-6.6971	0.5116	35	-12.0517	-12.4438	0.3921
6	-1.8964	-1.8646	-0.0318	21	-0.5055	-0.5660	0.0604	36	-4.1520	-4.9714	0.8195
7	-0.3035	-0.3763	0.0728	22	-1.2734	-1.5743	0.3009	37	-2.8187	-3.7045	0.8858
8	-3.8576	-2.6669	-1.1906	23	-13.0454	-13.1254	0.0800	38	-5.9380	-6.4168	0.4788
9	-0.7708	-0.9622	0.1914	24	-1.0798	-1.3272	0.2474	39	-5.1366	-5.8268	0.6902
10	-0.7273	-1.1595	0.4322	25	-0.9576	-0.9388	-0.0188	40	-8.1119	-8.2823	0.1705
11	-0.9400	-0.9388	-0.0013	26	-2.4400	-2.3274	-0.1126	41	-15.7438	-15.5705	-0.1732
12	-0.8333	-0.8452	0.0119	27	-8.6949	-8.4722	-0.2228	42	-1.6239	-1.9121	0.2881
13	-14.0380	-14.3980	0.3600	28	-0.5921	-0.7123	0.1202	43	-0.8323	-0.8452	0.0129
14	-20.4151	-21.8048	1.3897	29	-0.4830	-0.5904	0.1074	44	-1.0124	-0.9388	-0.0737
15	-36.0105	-39.7264	3.7159	30	-2.2561	-2.2777	0.0216	45	-20.0269	-20.2263	0.1993

TABLE 4. A Comparison of the proposed antenna to existing work.

References	Size $(\mathbf{mm}^2)$	No of notch	ML prediction	Notch Freq (GHz)	Max Insertion loss	Max η (%)	Peak Gain (dBi)
[6]	32×27	2	No	2.4, 5.2	-0.9 dB,	79	9.5
[7]	36×36	3	No	3.5, 5.5, 7.5	-3.5 dB	94.5	4.7
[9]	40×40	4	No	2.4, 3.5, 5.5, 8.2	-2.1 dB	-	4.5
[10]	15×15	2	No	1.58, 2.44	-5 dB,	52	2
[14]	24×35	1	No	5.5	-2.5 dB	95	3
[16]	150×150	1	No	3.1	-2.8 dB	78	7.1
[20]	120×120	1	No	5.8	-1.4 dB	79	6.6
[27]	30×25	5	No	2.67, 4.13, 5.31,	-1.2 dB	96	4.76
[28]	28×25	2	No	3.95, 9.38	-2.2 dB	-	6.1
[29]	30×25	3	No	3.5, 5.5, 8.1	-1.3 dB	78	5
This work	22×33	3	Yes	2, 3.2, 4.5	-0.4 dB	95.4	4.7

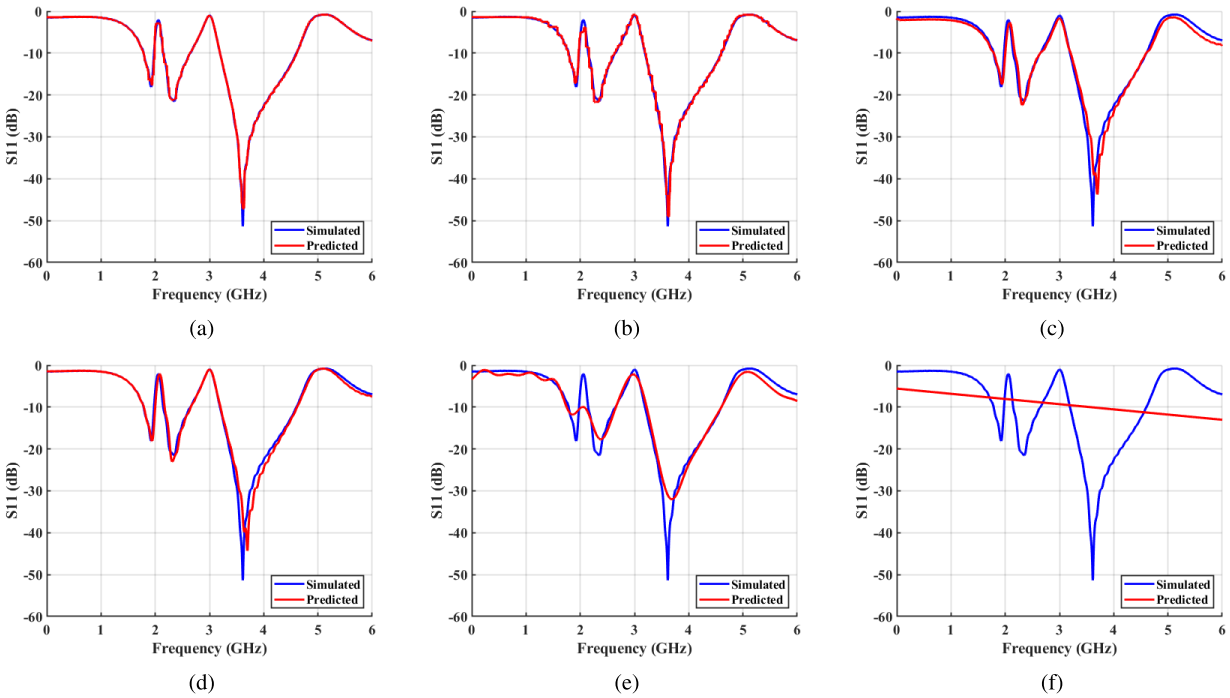

FIGURE 22. The simulated and predicted S_{11} *(dB)*; (a) Gaussian process regression, (b) Ensemble regression, (c) SVM regression. (d) Decision tree regression, (e) Kernel regression, (f) Efficient linear regression.

model the antenna from scratch using programs such as CST studio suit, HFSS, FEKO, or any other antenna design software. Significantly less time is needed for optimization with this prediction model than with traditional

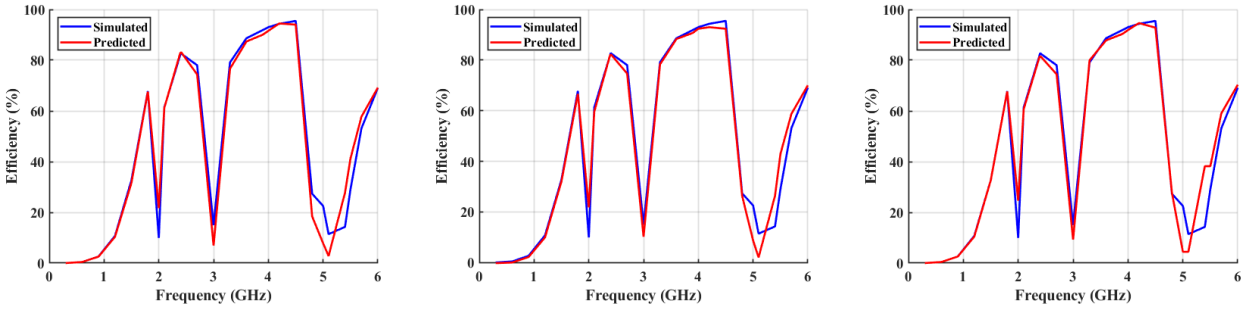

FIGURE 23. The simulated and predicted efficiency (%); (a) Gaussian process regression, (b) Ensemble regression, (c) SVM regression.

antenna design tools, which is another advantageous characteristic.

The performance of the proposed antenna is shown in Table 4 concerning size, number of notches, maximum insertion loss, efficiency, gain, and other factors. Except for [10], it is evident from the figure that the proposed antenna is comparatively smaller in size than the others. In a similar vein, the Insertion Loss (IL), for which the proposed structure demonstrated a value less than 0.5 *dB*, surpassed all others. Nonetheless, its efficiency and gain are moderate. The proposed structure has the same peak gain as shown in [7], a lower IL than all, and a greater efficiency than [29] when compared to references [7] and [29], which have the same number of notches. In addition to these advantages of the proposed design, the antenna's S_{11} and efficiency were predicted using a machine learning prediction technique.

IX. CONCLUSION

This paper described a wideband (WB) antenna fed by a microstrip with filtering notches. Within its coverage region, the antenna is designed to eliminate interference in three separate bands. To do this, three notch bands are formed by adding U, L, and C-shaped features into the WB antenna's feeding line and radiating patch. The proposed antenna's radiation pattern, gain, and reflection coefficient S11 < -10 dB were measured experimentally and found to be consistent with simulated findings. One of the proposed antenna's most notable features is its multiband coverage, which includes 1.9 GHz, 2.3 GHz, and 3.5 GHz. ADS schematic and machine learning algorithms were used to further validate the results. Because of its versatility, the antenna is suitable for a wide range of applications requiring a multiband solution. Furthermore, the proposed antenna has a desirable peak gain of 4.7 dBi and a maximum attenuation level of -0.4 dBi, making it ideal for suppression of interference in long-distance communication and signal reception in locations with low signal levels.

ACKNOWLEDGMENT

The authors would like to thank Al-Kharj, Prince Sattam bin Abdulaziz University, Saudi Arabia, for providing some of the research tools used in this investigation.

REFERENCES

[1] R. Saraswat, "A hybrid fractal metamaterial inspired multiband antenna for wireless applications," *Wireless Pers. Commun.*, vol. 124, no. 3, pp. 2593–2612, 2022.

[2] L.-R. Tan, C. Yanhuan, W. Duan, and Z. Li, "Coplanar waveguide fed roof-shaped multiband antenna for WPAN applications," in *Proc. 5th Int. Conf. Circuits, Syst. Simul. (ICCSS)*, May 2022, pp. 146–150.

[3] R. Kumar, S. Singh, and A. Chauhan, "Multiband antenna design based on Gosper fractal for implantable biomedical devices," *Int. J. Microw. Wireless Technol.*, vol. 14, no. 8, pp. 970–980, 2022.

[4] H. So and K. Maruta, "Sector design using multiband antenna with metamaterial reflector for cellular UAV system," *IEEE Access*, vol. 10, pp. 4924–4933, 2022.

[5] B. Fady, J. Terhzaz, A. Tribak, F. Riouch, and A. Mediavilla, "Novel miniaturized planar low-cost multiband antenna for industry 4.0 communications," *Prog. Electromagn. Res. C*, vol. 93, pp. 29–38, 2019.

[6] K. Zhang, Z. H. Jiang, W. L. Zhou, P. Peng, and W. Hong, "A compact, band-notched ultra-wideband fully-recessed antenna with pattern diversity for V2X communications," *IEEE Open J. Antennas Propag.*, vol. 3, pp. 1302–1312, 2022.

[7] S. Jayant and G. Srivastava, "Close-packed quad-element triple-band-notched UWB MIMO antenna with upgrading capability," *IEEE Trans. Antennas Propag.*, vol. 71, no. 1, pp. 353–360, Jan. 2023.

[8] K. Paracha, A. Butt, A. Alghamdi, S. Babale, and P. Soh, "Liquid metal antennas: Materials, fabrication and applications," *Sensors*, vol. 20, no. 1, p. 177, 2020.

[9] P. Jha, A. Kumar, A. De, and R. Jain, "CPW-fed metamaterial inspired compact multiband antenna for LTE/5G/WLAN communication," *Frequenz*, vol. 76, nos. 7–8, Mar. 2022.

[10] D. Kim, N. Jo, H. Jang, and C. Kim, "Design of the ultrawideband antenna with a quadruple-band rejection characteristics using a combination of the complementary split ring resonators," *Prog. Electromagn. Res.*, vol. 112, pp. 93–107, 2011.

[11] M. Alibakhshikenari, E. Limiti, M. Naser-Moghadasi, B. Virdee, and R. Sadeghzadeh, "A new wideband planar antenna with band-notch functionality at GPS, Bluetooth and WiFi bands for integration in portable wireless systems," *AEU Int. J. Electron. Commun.*, vol. 72, pp. 79–85, Feb. 2017.

[12] R. Azim, M. T. Islam, and A. T. Mobashsher, "Design of a dual band-notch UWB slot antenna by means of simple parasitic slits," *IEEE Antennas Wireless Propag. Lett.*, vol. 12, pp. 1412–1415, 2013.

[13] H. Qi and H. Liu, "Single-ended band-notched Vivaldi antenna with common mode suppression and low cross polarization," *IEEE Antennas Wireless Propag. Lett.*, vol. 20, no. 10, pp. 1983–1987, Oct. 2021.

[14] T. Ma and S. Wu, "Ultrawideband band-notched folded strip monopole antenna," *IEEE Trans. Antennas Propag.*, vol. 55, no. 9, pp. 2473–2479, Sep. 2007.

[15] C. Hong, C. Ling, I. Tarn, and S. Chung, "Design of a planar ultrawideband antenna with a new band-notch structure," *IEEE Trans. Antennas Propag.*, vol. 55, no. 12, pp. 3391–3397, Dec. 2007.

[16] J. Li, H. Chen, J. Wang, S. Li, X. Yin, and H. Zhao, "Ultrawideband antipodal tapered slot antenna with reflectionless notched band," *IEEE Antennas Wireless Propag. Lett.*, vol. 21, no. 3, pp. 431–435, Mar. 2022.

[17] Z. Li, J. Han, Y. Mu, X. Gao, and L. Li, "Dual-band dual-polarized base station antenna with a notch band for 2/3/4/5G communication systems," *IEEE Antennas Wireless Propag. Lett.*, vol. 19, no. 12, pp. 2462–2466, Dec. 2020.

[18] S. Fu, Z. Cao, X. Quan, and C. Xu, "A broadband dual-polarized notched-band antenna for 2/3/4/5G base station," *IEEE Antennas Wireless Propag. Lett.*, vol. 19, no. 1, pp. 69–73, Jan. 2020.

[19] C. G. Hynes and R. G. Vaughan, "Conical monopole antenna with integrated tunable notch filters," *IEEE Antennas Wireless Propag. Lett.*, vol. 19, no. 12, pp. 2398–2402, Dec. 2020.

[20] D. Azra, "Design of compact monopole antenna with u-shaped defected ground structure (DGS) for UWB application," *J. Telecommun., Electron. Comput. Eng.*, vol. 14, no. 3, pp. 11–15, 2022.

[21] K. Wong, Y. Chi, C. Su, and F. Chang, "Band-notched ultra-wideband circular-disk monopole antenna with an arc-shaped slot," *Microw. Opt. Technol. Lett.*, vol. 45, no. 3, pp. 188–191, 2005.

[22] C. Huang and W. Hsia, "Planar ultra-wideband antenna with a frequency notch characteristic," *Microw. Opt. Technol. Lett.*, vol. 49, no. 2, pp. 316–320, 2007.

[23] J. Jang and H. Hwang, "An improved band-rejection UWB antenna with resonant patches and a slot," *IEEE Antennas Wireless Propag. Lett.*, vol. 8, pp. 299–302, 2009.

[24] W.-S. Lee, D.-Z. Kim, K.-J. Kim, and J.-W. Yu, "Wideband planar monopole antennas with dual band-notched characteristics," *IEEE Trans. Microw. Theory Techn.*, vol. 54, no. 6, pp. 2800–2806, Jun. 2006.

[25] H.-T. Hu, B.-J. Chen, and C. H. Chan, "A transparent proximity-coupled-fed patch antenna with enhanced bandwidth and filtering response," *IEEE Access*, vol. 9, pp. 32774–32780, 2021.

[26] D. Potti, Y. Tusharika, M. G. N. Alsath, S. Kirubaveni, M. Kanagasabai, R. Sankararajan, S. Narendhiran, and P. B. Bhargav, "A novel optically transparent UWB antenna for automotive MIMO communications," *IEEE Trans. Antennas Propag.*, vol. 69, no. 7, pp. 3821–3828, Jul. 2021.

[27] Z. Deng, C. Lai, Y. Wang, and K. Deng, "Design of a quadruple band-notched ultra-wideband (UWB) antenna using curled C-shaped structures and interdigital inductance slots," *Electronics*, vol. 11, no. 23, p. 3949, 2022.

[28] Z. Zhao, "A miniaturized wearable antenna with five band-notched characteristics for medical applications," *IEEE Antennas Wireless Propag. Lett.*, vol. 22, no. 6, pp. 1246–1250, Sep. 2023.

[29] J. Wu and J. Li, "Compact ultra-wideband antenna with 3.5/5.5 GHz dual band-notched characteristic," in *Proc. 5th IEEE Int. Symp. Microw., Antenna, Propag. EMC Technol. for Wireless Commun.*, Oct. 2013, pp. 446–450.

[30] J. Deng, Y. Yin, S. Zhou, and Q. Liu, "Compact ultra-wideband antenna with tri-band notched characteristic," *Electron. Lett.*, vol. 44, no. 21, pp. 1231–1233, 2008.

[31] R. Zaker, C. Ghobadi, and J. Nourinia, "Bandwidth enhancement of novel compact single and dual band-notched printed monopole antenna with a pair of l-shaped slots," *IEEE Trans. Antennas Propag.*, vol. 57, no. 12, pp. 3978–3983, May 2009.

[32] L. Cai, Y. Li, G. Zeng, and H. Yang, "Compact wideband antenna with double-fed structure having band-notched characteristics," *Electron. Lett.*, vol. 46, no. 23, pp. 1534–1536, 2010.

[33] M.-C. Tang, S. Xiao, T. Deng, D. Wang, J. Guan, B. Wang, and G.-D. Ge, "Compact UWB antenna with multiple band-notches for Wimax and WLAN," *IEEE Trans. Antennas Propag.*, vol. 59, no. 4, pp. 1372–1376, Apr. 2011.

[34] X. Liao, H. Yang, N. Han, and Y. Li, "Aperture UWB antenna with triple band-notched characteristics," *Electron. Lett.*, vol. 47, no. 2, pp. 77–79, 2011.

[35] C. Yu, W. Hong, L. Chiu, G. Zhai, C. Yu, W. Qin, and Z. Kuai, "Ultrawideband printed log-periodic dipole antenna with multiple notched bands," *IEEE Trans. Antennas Propag.*, vol. 59, no. 3, pp. 725–732, Mar. 2011.

[36] B. Rahmati and H. Hassani, "Wideband planar plate monopole antenna with dual tunable notch," *Electron. Lett.*, vol. 46, no. 7, pp. 480–481, 2010.

[37] B. Rahmati and H. Hassani, "Multi-notch slot loaded wide band planar plate monopole antenna," *IET Microw., Antennas Propag.*, vol. 4, no. 12, pp. 2160–2165, 2011.

[38] F. Yu and C. Wang, "Design of a CPW-fed dual band-notched planar wideband antenna for UWB applications," in *Ultra Wideband Communications: Novel Trends—Antennas and Propagation*. Rijeka, Croatia: InTech, 2010.

[39] W. Balani, M. Sarvagya, A. Samasgikar, T. Ali, and P. Kumar, "Design and analysis of super wideband antenna for microwave applications," *Sensors*, vol. 21, no. 2, p. 477, 2021.

[40] U. Musa, S. Babani, S. Babale, A. Ali, Z. Yunusa, and S. Lawan, "Bandwidth enhancement of millimeter-wave microstrip patch antenna array for 5G mobile communication networks," *Bull. Electr. Eng. Informat.*, vol. 12, no. 4, pp. 2203–2211, 2023.

[41] W. Gibson, *The Method of Moments in Electromagnetics*. Boca Raton, FL, USA: CRC Press.

[42] M. Yahya, S. Soeung, S. Rahim, U. Musa, S. Hashwan, and M. A. Haque, "Machine learning-optimized compact frequency reconfigurable antenna with RSSI enhancement for long-range applications," *IEEE Access*, vol. 12, pp. 10970–10987, 2024.

[43] Z. Abideen, "Analysis of enrollment criteria in secondary schools using machine learning and data mining approach," *Electronics*, vol. 12, no. 3, p. 694, 2023.

[44] *Statistics and Machine Learning Toolbox*, TM Inc, MathWorks, Natick, MA, USA, Mar. 2024.

[45] U. Bhattacherjee, C. K. Anjinappa, L. Smith, E. Ozturk, and I. Guvenc, "Localization with deep neural networks using mmWave ray tracing simulations," in *Proc. SoutheastCon*, Mar. 2020, pp. 1–8.

[46] G. James, D. Witten, T. Hastie, R. Tibshirani, and J. Taylor, "Linear regression," in *An Introduction to Statistical Learning*. Cham, Switzerland: Springer, Jul. 2023, pp. 69–134.

[47] J. Wu and H. Yang, "Linear regression-based efficient SVM learning for large-scale classification," *IEEE Trans. Neural Netw. Learn. Syst.*, vol. 26, no. 10, pp. 2357–2369, Oct. 2015.

[48] B. Ville, "Decision trees," *Wiley Interdiscipl. Rev., Comput. Statist.*, vol. 5, no. 6, pp. 448–455, Dec. 2013.

[49] D. Meyer and F. T. Wien, "Support vector machines," *R News*, vol. 1, no. 3, pp. 23–26, 2001.

[50] E. Schulz, M. Speekenbrink, and A. Krause, "A tutorial on Gaussian process regression: Modelling, exploring, and exploiting functions," *J. Math. Psychol.*, vol. 85, pp. 1–16, Aug. 2018.

[51] M. Schuld, "Supervised quantum machine learning models are kernel methods," 2021, *arXiv:2101.11020*.

[52] P. Kazienko, E. Lughofer, and B. Trawinski, "Hybrid and ensemble methods in machine learning," *J. Universal Comput. Sci.*, vol. 19, no. 4, p. 146, 2013.

[53] S. A. Shetty, T. Padmashree, B. M. Sagar, and N. K. Cauvery, "Performance analysis on machine learning algorithms with deep learning model for crop yield prediction," in *Data Intelligence and Cognitive Informatics*. Singapore: Springer, 2021, pp. 739–750.

SULEIMAN ALIYU BABALE (Member, IEEE) received the bachelor's degree in electrical engineering from Bayero University Kano, in 2005, the master's degree in electrical engineering from Ahmadu Bello University, Zaria, in 2012, and the Ph.D. degree in electrical engineering with a major in telecommunications from Universiti Teknologi Malaysia, in 2018. He is currently a Senior Lecturer with Bayero University Kano. He was a Postdoctoral Researcher with Multimedia University, Melaka, from February 2022 to February 2024. His research interests include the IoT, design and implementation of electronics components, antennas, sensors and microwave devices, power line communication, propagation, and wireless and mobile communications. He has over 50 publications on antenna design and wireless communications for 5G. He has received several grants and has been a member of the Council for the Regulation of Engineering in Nigeria (COREN), in 2011.

TAN KIM GEOK (Member, IEEE) received the B.E., M.E., and Ph.D. degrees in electrical engineering from Universiti Teknologi Malaysia, in 1995, 1997, and 2000, respectively. He was a Senior Research and Development Engineer with EPCOS Singapore, in 2000. From 2001 to 2003, he joined DoCoMo Euro-Laboratories, Munich, Germany. He is currently an Academic Staff with Multimedia University. His research interests include radio propagation for outdoor and indoor, RFID, multi-user detection techniques for multi-carrier technologies, and A-GPS.

SHARUL KAMAL ABDUL RAHIM (Fellow, IEEE) received the degree in electrical engineering from the University of Tennessee, USA, in 1996, the M.Sc. degree in engineering (communication engineering) from Universiti Teknologi Malaysia (UTM), in 2001, and the Ph.D. degree in wireless communication system from the University of Birmingham, U.K., in 2007. He is currently a Professor with the Wireless Communication Centre, Faculty of Electrical Engineering, UTM Skudai. He has published more than 50 journal articles and technical proceedings on rain attenuations, smart antenna systems, microwave design, and reconfigurable antenna in national; and international journals and conferences. His research interest includes smart antenna on communication systems. He is a member of the IEEE Malaysia Section, the Member Board of Engineer Malaysia, the Institute of Engineer Malaysia, and the Eta Kappa Nu Chapter (International Electrical Engineering Honor Society, University of Tennessee).

CHIA PAO LIEW received the Ph.D. degree in engineering education from Universiti Teknologi Malaysia and the master's degree in electronics (communication systems) from the University of Hertfordshire, U.K. He is currently the Assistant Dean and an Assistant Professor with the School of Energy and Chemical Engineering, Xiamen University Malaysia. His publications include refereed journals and conference papers in the domains of engineering education and wireless communication.

UMAR MUSA (Student Member, IEEE) received the bachelor's degree in electrical engineering from Bayero University Kano, Nigeria, in 2012, and the M.Eng. degree in electronic and telecommunication engineering from Universiti Teknologi Malaysia (UTM), Malaysia, in 2016. He is currently pursuing the Ph.D. degree with the Department of Communication Engineering, Faculty of Electrical and Electronic Engineering, Universiti Tun Hussein Onn Malaysia (UTHM). He is currently a Lecturer with the Department of Electrical Engineering, Bayero University Kano. His research interests include but are not limited to, the design of RF and microwave devices, and active antennas measurement. He has been a member of the Council for the Regulation of Engineering of Nigeria, since 2019.

MUKHTAR FATIHU HAMZA received the bachelor's and master's degrees in electrical engineering from Bayero University Kano, in 2008 and 2013, respectively, and the Ph.D. degree in automation, control and robotics from the University of Malaya, Malaysia, in 2017. He was a Postdoctoral Research Fellow with the University of Malaya, Malaysia, in 2019. Currently, he is an Assistant Professor with The Department of Mechanical Engineering, Prince Sattam bin Abdulaziz University, Saudi Arabia.

YASER AWADH BAKHURAISA received the B.Eng. degree in electronic engineering from Hadhramout University of Science & Technology, Hadhramout, Yemen, in 2009, and the masters' degree in electronics engineering with major in electronic systems from Universit Teknical Malaysia (UTeM), in 2019. He is currently pursuing the Ph.D. degree in asynchronous V2V with non-line of sight (NLoS) vehicular sensing. His current research interests include vehicular localization, geometrical positioning, and radio propagation.

LI LI LIM (Senior Member, IEEE) received the Advanced Diploma degree in technology (electronics engineering) from the Tunku Abdul Rahman College (TARC), the M.Sc. degree in electronics from the Queen's University of Belfast, and the Ph.D. degree in electrical and electronics engineering from the University of Nottingham, Malaysia, in the area of MIMO channel coding and equalization, in 2019. Her current research interests include statistical signal and image processing, machine learning, and next-generation wireless communication signal processing.